Int. J. Electrochem. Sci., 17 **(2022)** Article Number: 221245, doi: 10.20964/2022.12.46

International Journal of
ELECTROCHEMICAL
SCIENCE
www.electrochemsci.org

Mini review

Progress in the design and application of magnetic materials-based photoelectrochemical biosensors

Dan-Dan Liu, Yan-Biao Zhou, Kai-Tuo Du and Chang-Dong Chen**

College of Chemistry and Environmental Engineering, Pingdingshan University, Pingdingshan, Henan 467000, People's Republic of China
*E-mail: liudd0811@126.com (D.L.); qgfenghxx@163.com (C.C.)

Received: 1 October 2022 / *Accepted:* 14 November 2022 / *Published:* 30 November 2022

The conventional photoelectrochemical (PEC) biosensors usually require the immobilization of recognition elements on the electrode surface by physical adsorption, embedding, self-assembly or covalent bonding. However, such biosensors are limited in practical applications because the modified electrode can only be used once. Magnetic-assisted biosensors have significant advantages in separation and preconcentration of analytes in complex samples. More importantly, the magnetic sensing systems show high-throughput since magnetic materials can be produced and preserved in a large-scale dose. In this work, we review the progress in the design and application of magnetic-assisted PEC biosensors based on the different functions of magnetic materials in the sensing systems.

Keywords: photoelectrochemical biosensors; magnetic biosensors; signal labels; high-throughput

1. INTRODUCTION

Photoelectrochemical (PEC) biosensors based on photoelectric effect are a type of new sensing technologies, which have attracted extensive attention in different fields. In the general PEC detection system, the external light is the source of excitation and the photocurrent is the output signal. The techniques refer to two completely different input and output physical quantities, thus avoiding the interference from the excitation source [1]. In this method, the electrons hole pairs will be generated when the photosensitive materials are excited by light. The generated electrons transfer onto the electrode surface, thus realizing the conversion of light energy to electrical energy and producing a photocurrent. The combination of spectral analysis and electrochemical analysis provides a basis for the development and application of a variety of PEC biosensors, and endows the sensing platforms a variety of advantages, including low background signal, high sensitivity, low cost, easy miniaturization and portability, and real-time detection [2]. To date, PEC biosensors have been developed for the detection

of different targets, and at least a thousand scientific papers about PEC sensing have been reported. The analytes refer to ions, small molecules, DNA, proteins, cells, and even organisms [2-4]. In order to realize the practical applications of biosensors, one of the most critical issues is to design a high-throughput sensing system suitable for large-scale production. Traditional PEC biosensors require the immobilization of recognition elements on the electrode surface by physical adsorption, embedding, self-assembly or covalent bonding, but the pretreatment and reuse of the electrode in this way are cumbersome and time-consuming. Moreover, it is difficult to achieve high-throughput analysis due to the limitation of electrode.

Magnetic beads (MBs) can be used as the support materials and separation tools for preconcentration and purification of analytes through the specific molecular interaction. Recently, the recognition elements such as antibodies, nucleic acids and polypeptides have been immobilized on the surface of MBs to develop various biosensors [5-7]. The magnetic sensing strategies exhibit the advantages of separation and preconcentration of targets in complex samples under an external magnetic field, thus decreasing the background interferences and showing high sensitivity and selectivity. Moreover, MBs can be used as the signal labels to increase the detection sensitivity. In this review, we summarized the progress in the design and application of magnetic-assisted PEC biosensors based on the difference in the functions of MBs within the sensing systems.

2. MAGNETIC-ASSISTED PEC BIOSENSORS

2.1 Carriers for separation and preconcentration of targets

MBs with functional groups (e.g. –COOH and $–NH_2$) can be utilized to decorate the electrode for the immobilization, separation and preconcentration of biomolecules [8-10], thus facilitating the design of PEC biosensors. For example, Chen et al. reported the PEC detection of histone acetyltransferase (HAT) by using BiOI nanoflower as the photoactive material and ZnO QDs as the photocurrent inhibitors [11]. In this work, the aminated Fe_3O_4 nanoparticles were used as the linkers to immobilize 3-maleimidopropionic acid (MIPA) and capture the produced coenzyme A (CoA) on the electrode. Then, ZnO QDs were attached onto the electrode by binding with the captured CoA, thus leading to the decrease in the photocurrent. By monitoring the produced CoA by PEC biosensor, HAT has been determined in the concentration range of 0.01 ~ 500 nM.

More commonly, MBs can be employed as the solid-phase for the biological recognition and magnetic separation of targets from real complex samples, which can remove the coexisting species. Then, the target-captured MBs can be immobilized on the electrode surface with the aid of the magnet [12]. The use of MBs can achieve the reusable electrode surface and improve the sensitivity of PEC biosensors. Moreover, the detection time in MBs-based assays is lower than that of the electrode-based assays because the recognition process happens in suspension. To avoid the use of enzyme labels or molecule tags, label-free techniques based on various detection mechanisms can be developed to monitor the interaction between recognition elements and targets. Li et al. designed a PEC biosensor for progesterone detection based on Fe_3O_4@SiO_2@TiO_2 magnetic−optical bifunctional beacon [13]. As shown in Figure 1, the superparamagnetic Fe_3O_4 nanoparticles were capped by SiO_2 and TiO_2 shell

(Fe_3O_4@SiO_2@TiO_2) and then aminated for the functionalization of aptamer and capture probe DNA. The capture of target by the chain-structured aptamer-modified Fe_3O_4@SiO_2@TiO_2 induced the conformation change of the aptamer. The target-covered Fe_3O_4@SiO_2@TiO_2 blocked the incident light and decreased the photocurrent. Furthermore, Zeng et al. demonstrated that the immobilization of cancer cells captured by the MBs on the electrode could decrease the PEC signal [14].

Table 1. Detection performances of different PEC biosensors by using MBs for separation and concentration of targets.

Signal labels	Target	Linear ranges	LOD	Ref.
Fe_3O_4@SiO_2@TiO_2	progesterone	0 ~ 10 nM	0.3 pM	[13]
BTA-C4Ph-PM6	MCF-7	50 ~ 10000 cell/mL	41 cell/mL	[14]
TiO_2-AgNPs	MMP-2	1 fg/mL ~ 100 pg/mL	0.34 fg/mL	[15]
CdSe QDs	microRNA-155	10 aM ~ 10 pM	3.2 aM	[16]
CdTe QDs/ssDNA-Fe_3O_4@SiO_2	CEA	10 fg/mL ~ 1 ng/mL	3.98 fg/mL	[17]
Aptamer-AuNPs	MCF-7	10 ~ 10000 cell/mL	9 cell/mL	[18]
Ag_2S nanocrystals	MCF-7	10 ~ 5000 cell/mL	3 cell/mL	[19]
Cu_2O NPs	MCF-7	3 ~ 3000 cell/mL	1 cell/mL	[20]
Co_3O_4-AAO	HER2	1 pg/mL ~ 1 ng/mL	26 fg/mL	[21]
dC_{20}-modified AuNPs	NFL	5 pg/mL ~ 10 ng/mL	2 pg/mL	[22]
TiO_2-g-C_3N_4-PMA	PSA	0.01 ~ 50 ng/mL	6.25 pg/mL	[23]

Abbreviation: MCF-7, Michigan Cancer Foundation-7; MMP-2, matrix metalloproteinase-2; HER2, human epidermal growth factor receptor 2; CEA, carcinoembryonic antigen; PSA, prostate-specific antigen; NFL, neuroflament light chain.

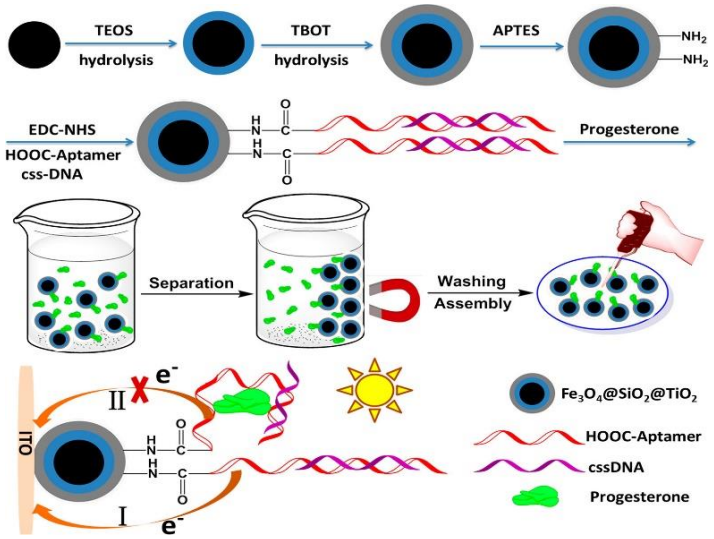

Figure 1. Schematic illustrations for the synthesis of Fe_3O_4@SiO_2@TiO_2 modified with aptamer and capture DNA for PEC aptasensing of progesterone. Reproduced with permission [13]. Copyright 2020, American Chemical Society.

Photoactive materials have been extensively used as signal labels owing to their excellent photoelectric properties [24]. For example, Li et al. used TiO_2-AgNPs as the plasmonic photoelectric beacon to label the detection antibody (Ab_2) for the detection of matrix metalloproteinase-2 [15]. AgNPs confined in amorphous TiO_2 shells could generate the electrons in situ, thus amplifying the photocurrent

response. Chen et al. developed a PEC biosensor for microRNA-155 detection by using waste-free entropy-driven DNA nanomachine on superparamagnetic Fe_3O_4@SiO_2 particles and CdSe QDs as signal labels [16]. Recently, a photocurrent polarity switching strategy has been developed to eliminate false-positive or false-negative signals in "signal-on" detection mode. For example, Mo et al. reported a signal-reversal-mode PEC biosensor by using superparamagnetic Fe_3O_4@SiO_2 to anchor dsDNA for the insertion of methylene blue [17]. As shown in Figure 2, the CdTe QDs-probe ssDNA-Fe_3O_4@SiO_2 could produce a photocathode current. In the present of carcinoembryonic antigen (CEA), Exo III-assisted cyclic amplification was promoted to produce a large number of output DNAs. The produced output DNAs were then captured by CdTe QD_S-probe ssDNA-Fe_3O_4@SiO_2 through hybridization reaction, allowing for the insertion of methylene blue molecules and producing a photoanode current under the same conditions. Plasmonic AuNPs and AgNPs can increase the photocurrent intensity by improving the absorption of light and broadening the absorption range. Therefore, they have been used as the labels to enhance the PEC signal. Recently, Luo et al. reported the PEC detection of Michigan Cancer Foundation-7 (MCF-7) cells with silver-stained AuNPs as the signal tags to enhance the photocurrent response [18]. The CTCs were captured by antibody-modified MBs and then concentrated on the photoactive matrix of organic PM6:Y6 p-n heterojunction. Then, the aptamer-modified AuNPs were added to label MCF-7 cells, thus initiating the occurrence of AuNPs-based silver staining reaction and leading to the increase of PEC response.

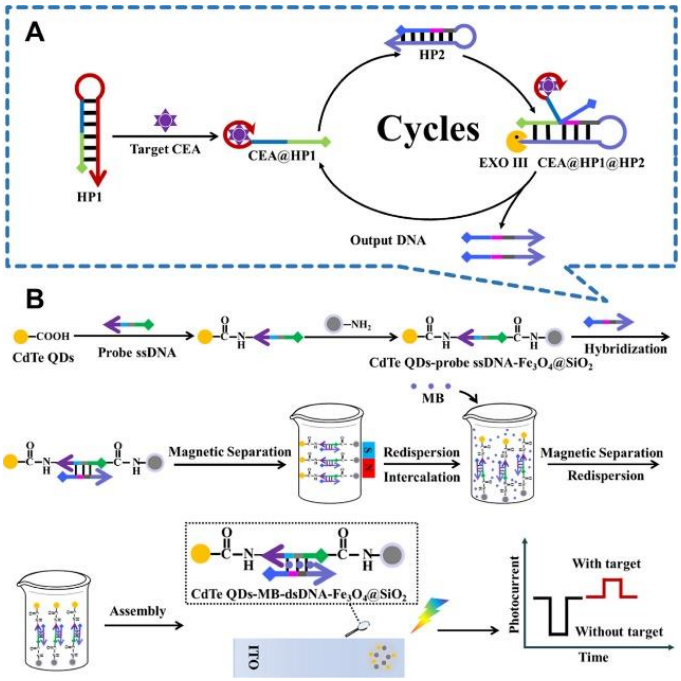

Figure 2. Schematic illustrations for the Exo III-assisted cyclic amplification signal (A) reversal-based PEC aptasensor (B). Reproduced with permission [17]. Copyright 2021, American Chemical Society.

Nanomaterials can be used as signal labels to reduce the photocurrent intensity by consuming the excitation energy or the electron donors for signal amplification [19]. Luo et al. reported a PEC biosensor

by using hexagonal carbon nitride tubes (HCNT) as the photoactive electrode materials [20]. The target circulating tumor cells (CTCs) were captured by magnetic Fe_3O_4 nanospheres via the antigen-antibody interaction. The aptamer-labeled Cu_2O nanoparticles were used as the signal tags. The formation of sandwich immunocomplexes caused the decrease in the photocurrent intensity of HCNT due to the steric hindrance of aptamer and the competition between Cu_2O and HCNT to absorb the exciting light. Meanwhile, Luo et al. used ascorbic acid oxidase (AAO)-modified Co_3O_4 nanoparticles as signal labels for the detection of human epidermal growth factor receptor 2 [21]. Co_3O_4 nanoparticles competed with HCNT for the adsorption of the excitation energy, and AAO caused the consumption of the electron donor (AA). Besides, Wang used aptamer-Ag_2S nanocrystals as competitive labels for the determination of MCF-7 cells [19]. Chen et al. reported a PEC biosensor for the detection of serum neuroflament light chain, in which the polycytosine DNA sequence on AuNPs acted as the template to form molybdophosphate precipitate on the electrode surface, reducing the photoelectrochemical current intensity [22].

The employment of electrochemical workstations and physical light sources makes the construction of PEC sensing platform complex, which may limit the application of PEC biosensors. For this view, self-powered chemiluminescence has been used to replace physical light sources and facilitate the portability and miniaturization of detection device. For instance, Yu et al. reported a portable magnetic-assisted self-powered PEC biosensor for the detection of prostate-specific antigen (PSA). The platform was integrated by self-powered photoelectric signal output and phosphomolybdic acid (PMA)-based photochromic visualization [23]. As shown in Figure 3, TiO_2-g-C_3N_4-PMA was utilized as the photosensitive material to modify the sensor chip. The N-(4-aminobutyl)-N-ethylisoluminol-modified AuNP was used for the signal output and amplification. After the immunoreaction, the chemiluminescence signal was intensified and the color of PMA-covered photochromic device changed from light yellow to heteropoly blue.

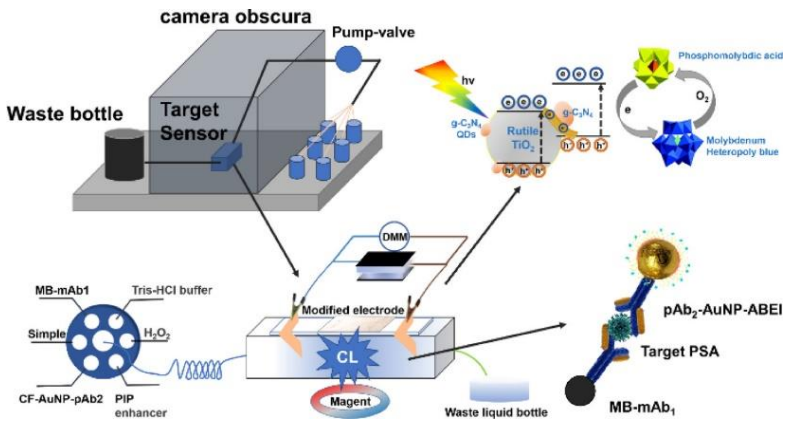

Figure 3. Schematic illustrations for the PE and the paper-based supercapacitor and the DMM readout of the PEC immunoassay model for PSA detection by the sandwich immunoassay. Reproduced with permission [23]. Copyright 2021, American Chemical Society.

2.2 Magnetic-assisted homogeneous reaction and target conversion

To improve the sensitivity of PEC biosensors, different nanomaterials have been used to load

small organic molecules. The loaded species could be released to modulate the photocurrent. For example, Ding et al. reported a PEC immunosensor with Fe_3O_4 nanosphere as the support of capture antibody and eosin Y-loaded $CaCO_3$ nanosphere as the signal label [25]. After the immune-reaction, the $CaCO_3$ nanosphere was dissolved by ethylene diamine tetraacetic acid (EDTA), leading to the release of eosin Y. The released eosin Y could sensitize the C_3N_4-MoS_2 semiconductor, thus producing an amplified photocurrent. Moreover, liposomes as an enclosed vesicles have been used to encapsulate different signal tracers (e.g. enzymes, quantum dots and electroactive species) for signal amplification. Lin et al. reported a competitive PEC immunosensor for Aflatoxin B_1 (AFB_1) detection with antibody-modified MB to capture the target and dopamine (DA)-loaded liposome (Figure 4) [26]. In this method, AFB1-bovine serum albumin (BSA) conjugates were covalently linked on the liposome surface with glutaraldehyde as the linker. The encapsulated DA molecules could be released from the liposome by Triton X-100. The released DA as the elector donor caused the increase in the photocurrent of Mn^{2+}-doped $Zn_3(OH)_2V_2O_7{\cdot}2H_2O$. However, the competitive binding between AFB1 and AFB1-BSA conjugate to the antibody-modified MB prevented the capture of DA-loaded liposome. As a result, a decreased PEC signal was observed. Furthermore, the liposomes-based PEC strategy has been used for the design of other PEC biosensors. For example, Gong et al. reported the PEC detection of human papilloma virus-related DNA by integration of DA-loaded liposome with CRISPR/Cas12a-mediated amplification strategy [27]. Zhang et al. reported a split-type PEC and electrochemical dual-modal aptasensor for tumor necrosis factor-α detection based on the methylene blue-liposome-mediated signal amplification strategy [28]. Zeng et al. reported a PEC bioassay for the detection of target Kana using liposome to load glutathione [29]. In this study, glutathione released under the treatment of Triton X-100 could amplify the photocurrent of the In_2O_3–$ZnIn_2S_4$-modified electrode.

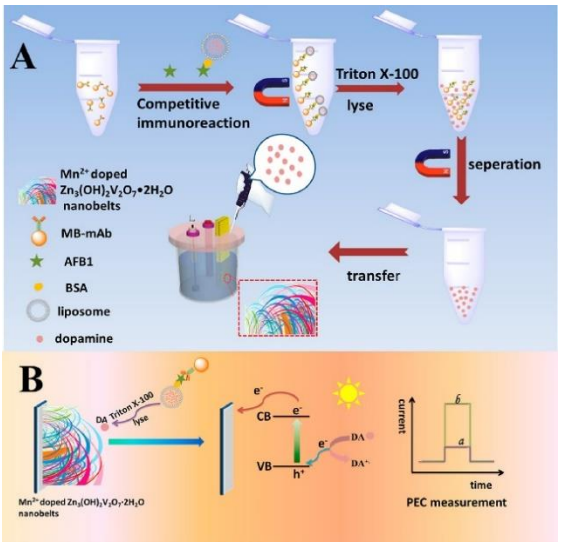

Figure 4. Schematic illustrations for Mn^{2+}-Doped $Zn_3(OH)_2V_2O_7{\bullet}2H_2O$ nanobelt-based PEC immunoassay for AFB_1. Reproduced with permission [26]. Copyright 2017, American Chemical Society.

Metal nanoparticles and nanoclusters (NCs) are always used as sacrificial tags to release

numerous metal ions for signal amplification [30]. Zhao et al. reported a PEC platform for the determination of adenosine based on AgNCs-assisted ion-exchange reaction with CdTe QDs [31]. In this method, adenosine initiated a cascade multiple cycling cleavage process with the aid of nicking endonuclease. The produced C-rich DNA could be captured by MBs to act as the template for the formation of AgNCs. Then, numerous Ag^+ ions released from AgNCs induced the ion−exchange with QDs and resulted in the increase of PEC current. Xia et al. developed a dual-modal aptasensor for exosome detection with copper oxide (CuO) nanoparticles as signal labels [32]. After the capture of exosomes by cholesterol DNA anchored on MBs through hydrophobic interaction, the aptamer-modified CuO nanoparticles were attached onto the surface of exosomes. Abundant Cu^{2+} ions were released from CuO nanoparticles to suppress the visible-light-induced oxidase mimic activity and PEC activity of 10-benzyl-2-amino-acridone.

Biomolecules can participate in the redox reaction at the PEC electrode surface to change the photocurrent. Qiu et al. reported a NIR responsive PEC biosensor based on core−shell NaYF4:Yb,Tm@TiO_2 upconversion microrods as the converter and target-triggered rolling circle amplification (RCA) [33]. As shown in Figure 5, after the formation of sandwich-type complex, the primer DNA was extended by RCA reaction. Then, the formed guanine (G)-rich DNA was cleaved by exonuclease I and exonuclease III and large amounts of free guanine bases were released to increase the photocurrent of unconversion microrods under NIR illumination. Lv et al. used the RCA reaction and DNA walker to generate free G bases for the detection of CEA, respectively [34, 35]. Besides, hemin and hemin/G-quadruplex complex can act as the electron acceptors to eliminate the photoelectrons generated from the photoactive matrix and to suppress the recombination of charges, eventually increasing the photocurrent. For this view, Lei et al. reported a magneto-controlled PEC biosensor for the determination of telomerase by using telomerase-extended G–rich DNA to remove hemin and recovery the PEC response [36]. Zhang et al. combined RCA with exonuclease III amplification to produce numerous hemin/G-quadruplex complexes that could enhance the photocurrent intensity [37].

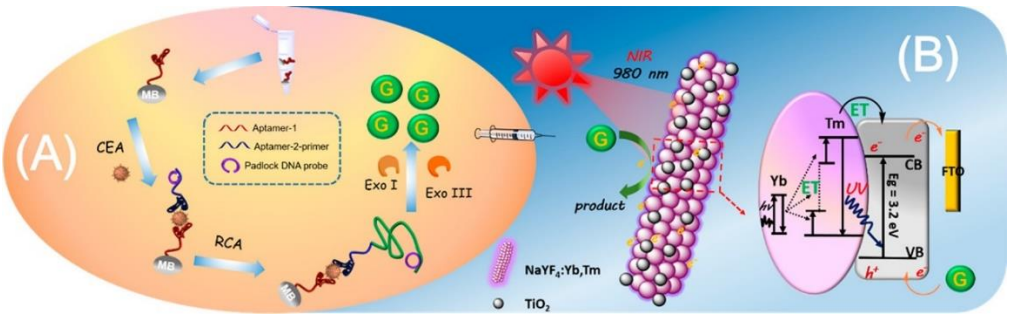

Figure 5. Schematic illustrations for NIR light-mediated PEC aptasensing platform for the detection of target CEA based on $NaYF_4$:Yb,Tm@TiO_2 upconversion microrods with RCA. Reproduced with permission [33]. Copyright 2018, American Chemical Society.

Nowadays, many effective PEC biosensors for the detection of DNA have been constructed with satisfactory results. Thus, by introducing MBs-based platform in homogeneous medium, various targets can be converted into DNA messengers to be detected by well-developed PEC methods [38-41].

Typically, Fu et al. reported a PEC biosensor for arsenate detection based on magnetic Co_3O_4−Fe_3O_4 cubes and the negative-background signal strategy [42]. In this study, the presence of arsenate could induce the generation of DNA messenger. Under the catalytic hairpin assembly (CHA) and hybridization chain reaction (HCR), a lot of G-quadruplexes were generated on the $AgInS_2$/ITO electrode. The immobilization of iron phthalocyanine can result in the switch of the photocurrent polarity from the anode to the cathode. Niu et al. proposed a magnetic-assisted PEC method for miRNA detection based on enzyme-assisted recycle amplification [43]. As shown in Figure 6, the electrode modified with 5,10,15,20-tetrakis (4-aminophenyl)-21H,23H-porphine (Tph-2H) showed a cathode photocurrent. The target could trigger the production of numerous output DNA strands through enzyme-assisted recycle amplification and strand-displacement strategy. The released output DNA could hybridize with hairpin DNA3 (HP3) on the electrode surface. Then, the HP3/output DNA duplex was digested by Exo III to induce the release of output DNA. Finally, the CdS QDs-modified hairpin DNA 4 (HP4) was captured by hybridization with the residual part of HP3, thus leading to a strong anodic photocurrent. Xia et al. designed a single-enzyme-assisted dual recycle amplification for miRNA-141 analysis by using SiO_2-labeled DNA as output messenger to decrease the PEC signal due to steric-hindrance effect of SiO_2 [44]. However, most of these methods require complex assembly steps and washing procedures, thus showing time-consuming and unstable defects. For this view, immobilization-free PEC biosensors are more attractive [45-47]. Li et al. designed a PEC sensing platform for miRNA detection based on programmable entropy-driven DNA amplifier and magnetic nanostructure [48]. As illustrated in Figure 7, the target miRNA initiated the DNA amplifier to produce a large number of output DNA strands. The released output DNA could open the partially hybridized dsDNA attached on the surface of Fe_3O_4@SiO_2 by chain replacement reaction, thus liberating the AuNPs-cDNA. After magnetic separation, the released AuNPs-cDNA could hybridize with CdSe/ZnS QDs-cDNA-1, thus leading to the decrease of photocurrent by the elegant exciton−plasmon interaction.

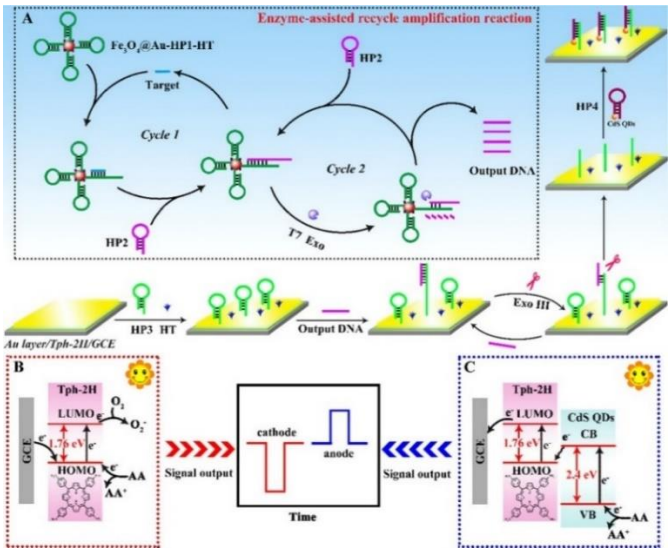

Figure 6. Schematic illustrations for the proposed PEC biosensor for miRNA-141 detection: T7 Exonuclease-assisted target recycle amplification process (A) and mechanism of electron transfer for cathode photocurrent generation (B) and anode photocurrent generation (C). Reproduced with permission [43]. Copyright 2021, American Chemical Society.

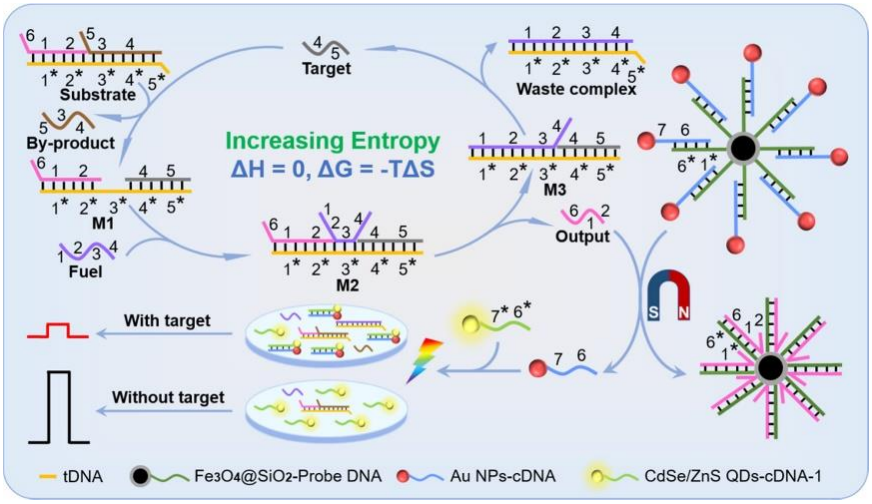

Figure 7. Schematic illustrations for the exciton−plasmon interaction-based PEC biosensor for miRNA-let-7a detection. Reproduced with permission [48]. Copyright 2021, American Chemical Society.

Enzyme-based signal amplification units have been widely utilized in PEC biosenosrs by integration with MBs-based homogeneous reaction. The presence of targets can induce the capture of enzymes on the MBs and the occurrence of hydrolysis or redox reactions. Then, the generated products are quantitatively measured by the nanomaterials-modified PEC electrode through different detection methods. For example, Zhou et al. developed a PEC sensing platform for PSA detection with rGO-$BiFeO_3$ as the photoactive material and glucose oxidase as the catalytic unit [49]. The interaction of aptamer and target induced the release of trigger DNA (tDNA) from the tDNA/aptamer duplex. The released tDNA was then captured by anchor DNA (aDNA)-modified MB (MB-aDNA). The unpaired part of tDNA could initiate the HCR with two glucose oxidase (GOx)-labeled hairpin DNA strands, thus producing a long dsDNA duplex with many GOx tags on the MB surface. The enzymatically produced H_2O_2 could consume the photoexcited electron from rGO-$BiFeO_3$, thus enhancing the photocurrent. In addition, Li et al. employed GOx-encapsulated DNA nanoflowers for signal amplification and the produced H_2O_2 could enhance the photocurrent on the GO-coated $Cu_{0.3}Zn_{0.7}O$ QDs-modified electrode [50].

Alkaline phosphatase (ALP) can hydrolyze the substrate ascorbic acid 2-phosphate (AAP) into reductive agent ascorbic acid (AA). The produced AA acting as the electron donor can be detected by a PEC technique [51-53]. Hao et al. developed a near-infrared light (NIR)-initiated PEC biosensor by coupling HCR with the ALP-based redox circle signal amplification [54]. As shown in Figure 8, the core−shell $NaYF_4$:Yb, Tm@$NaYF_4$ upconversion nanorods could generate the UV/vis light under 980 nm excitation and excite the TiO_2@CdS shell to produce photocurrent. In the presence of miRNA-133a, HCR reaction was triggered on the surface of MBs and many ALP-modified AuNPs were recruited. The produced AA could consume the photogenerated hole, and the oxidation product of dehydroascorbic acid (DHA) was reduced into AA through a tris-(2-carboxyethyl) phosphine (TCEP)-based chemical redox process, resulting in the enhanced photocurrent response. Zhu et al. reported a PEC and fluorescent dual-mode aptasensor for the assay of 17β-estradiol based on ALP-catalytic amplification [55]. In this study, the produced AA enhanced the PEC signal of the $CdIn_2S_4$ microspheres-modified electrode and

the declined dsDNA strands on the surface of MBs were quantified by the fluorescent indicator Helixyte Green™. Besides, Huang et al. used a G-quadruplex DNAzyme as the enzyme-mimic to design a proteinase-free dual-mode sensing strategy for the detection of kanamycin [56]. The G-quadruplex DNAzyme on the surface of MBs catalyzed the oxidation of hydroquinone into 1,4-benzoquinone, enhancing the photocurrent signal of the BiOI-modified electrode.

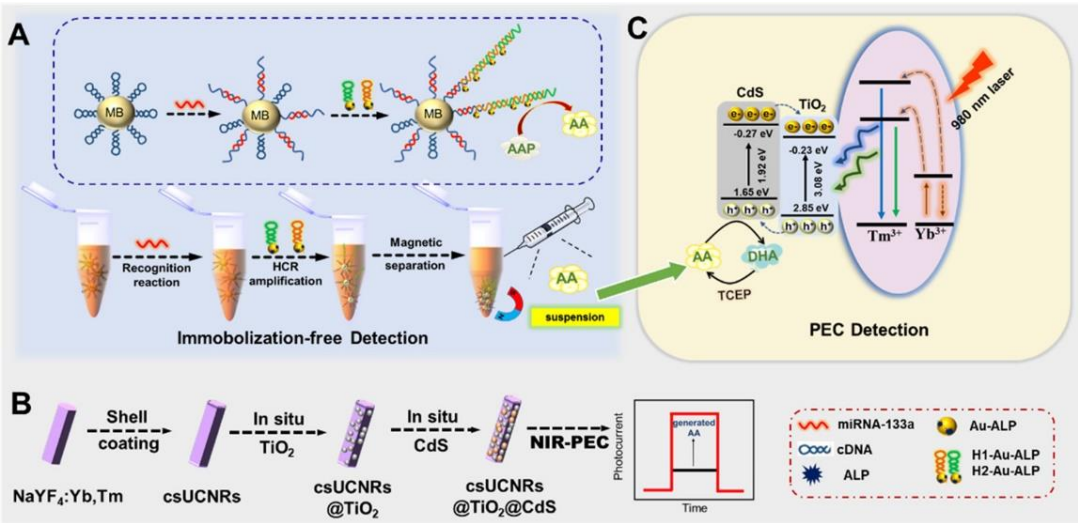

Figure 8. Schematic illustrations for the NIR-initiated PEC biosensor by coupling HCR with the ALP-based redox circle signal amplification. Reproduced with permission [54]. Copyright 2021, American Chemical Society.

Recently, the enzymatic product-induced etching reaction-based detection modes have been successfully integrated to develop split-type PEC sensing platforms. For example, Zeng reported a "signal-off" PEC immunosensor for CEA detection by using the product of horseradish peroxidase (HRP) to catalyze the etching reaction between H_2O_2 and the photoactive matrix (hollow cadmium sulfide) [57]. Lin et al. demonstrated that the product (H_2O_2) of GOx could etch/dissolve carbon QDs-modified MnO_2 nanosheets and thus developed a "signal-off" PEC immunosensing system for AFB_1 detection [58]. Zhang et al. designed a *magnetic-assisted* PEC aptasensor with $CuInS_2$-sensitized g-C_3N_4 as the photosensitive material and CoOOH as the light-blocking material [59]. The target was captured by the capture aptamer-modified MB, which allowed for the anchoring of trigger aptamer. Then, HCR with biotinylated hairpin DNA was initiated to produce a long dsDNA strand. Streptavidin-ALP (SA-ALP) was captured by the MB to produce a large number of AA, inducing the dissolution/etching of CoOOH nanosheet and recovering the photocurrent intensity. Su et al. developed a competitive PEC immunosensing platform for the detection of AFB_1 by using ALP-labeled AFB_1-BSA conjugate as the competitor [60]. Tang et al. presented a PEC biosensor for malathion detection by coupling RCA with butyrylcholinesterase (BChE)-mediated etching [61]. In this study, BChE accelerated the hydrolysis of acetylthiocholine into thiocholine (TCh), causing the dissolution of MnO_2 nanoflowers and the release of QDs from the electrode.

Table 2. Detection performances of different PEC biosensors by using MBs for homogeneous reaction and target conversion.

Signal labels	Target	Linear range	LOD	Ref.
EY@$CaCO_3$	CA724	0.05 mU/mL ~ 500 mU/mL	0.02 mU/mL	[25]
DA-loaded liposome	aflatoxin B_1	0.5 pg/mL ~ 10 ng/mL	0.3 pg/mL	[26]
DA-loaded liposome	HPV-16	5 pM ~ 100 nM	1.6 pM	[27]
Methylene blue-loaded liposome	TNF-α	5 fg/mL ~ 5 μg/mL	1.46 fg/mL	[28]
GSH-loaded liposome	kanamycin	0.1 5000 pM	22 fM	[29]
AgNCs	salivary cortisol	0.1 pg/mL ~ 100 ng/mL	0.06 pg/mL	[30]
AgNCs	adenosine	1.0 fM ~ 10 nM	0.5 fM	[31]
CuO NPs	exosome	5.00×10^3 ~ 1.00×10^6 particles/μL	1.38×10^3 particles/μL	[32]
$NaYF_4$:Yb,Tm@TiO_2	CEA	0.01 ~ 40 ng/mL	3.6 pg/mL	[33]
AuNPs	CEA	0.02 ~ 50 ng/mL	6.7 pg/mL	[34]
$NaYF_4$:Yb,Tm@ZnO	CEA	0.1 ~ 300 ng/mL	32 pg/mL	[35]
p-$CuBi_2O_4$ nanorod	telomerase	100 ~ 2000 HeLa cells	53 cells	[36]
Cu-doped $Zn_{0.3}Cd_{0.7}S$	PSA	0.05 ~ 40 ng/mL	16.3 pg/mL	[37]
CdS QDs	CEA	0.02 ~ 10 ng/mL	6.0 pg/mL	[38]
$AgInS_2$	arsenate	10 nM ~ 200 μM	1 nM	[42]
CdS QDs	miRNA-141	1 fM ~ 1 nM	0.33 fM	[43]
SiO_2	miRNA-141	0.25 fM ~ 2.5 nM	83 aM	[44]
CdTe QDs	miRNA-122	100 aM ~ 5 pM	94.2 aM	[45]
CdSe QDs	miRNA-20b	1 aM ~ 500 fM	0.36 aM	[46]
CdTe QDs	DNA	1 pM ~ 50 nM	0.76 pM	[47]
CdSe/ZnS QDs	miRNA-let-7a	10 aM ~ 1 pM	3.35 aM	[48]
GOx	PSA	0.001 ~ 100 ng/mL	0.31 pg/mL	[49]
ALP	PSA	0.02 ~ 40 ng/mL	Not reported	[51]
ALP	5-hmC	0.5 ~ 100 nM	0.16 nM	[52]
ALP	miRNA-21	1 fM ~ 1 nM	0.47 fM	[53]
ALP	miRNA-133a	0.1 fM ~ 1 nM	36.12 aM	[54]
ALP	17β-estradiol	0.1 ~ 200 nM	0.059 nM	[55]
G-DNAzymes	kanamycin	0.01 pg/mL ~ 1 ng/mL	0.55 fg/mL	[56]
HRP	CEA	0.02 ~ 50 ng/mL	6.12 pg/mL	[57]
GOx	Aflatoxin B_1	0.01 ~ 20 ng/mL	2.1 pg/mL	[58]
ALP	CEA	0.02 ~ 40 ng/mL	5.2 pg/mL	[59]
ALP	Aflatoxin B_1	0.01 ~ 10 ng/mL	2.6 pg/mL	[60]
Butyrylcholinesterase	malathion	0.001 ~ 100 ng/mL	0.68 pg/mL	[61]
ALP	PSA	5 pg/mL ~ 100 ng/mL	3.5 pg/mL	[62]
ALP	exosome	7.3×10^5 ~ 3.285×10^8 particles/mL	7.875×10^4 particles/mL	[63]
G-DNAzymes	malathion	0.001 ~ 1000 ng/mL	0.12 pg/mL	[64]
HRP	miRNA-21	0.01 pM ~ 10 nM	4.2 fM	[65]

Abbreviation: EY, eosin Y; CA724, carbohydrate antigen 724; HPV-16, human papilloma virus-related DNA; GSH, glutathione; TNF-α, tumor necrosis factor-α; AgNCs, silver nanoclusters; CEA, carcinoembryonic antigen; PSA, prostate-specific antigen; GOx, glucose oxidase; ALP, alkaline phosphatase; 5-hmC, 5-hydroxymethylcytosine; HRP, horseradish peroxidase.

Enzymatic products can be in-situ transformed into photoactive materials on the electrode to enhance the PEC performance. Recently, Xu et al. reported a magnetic-assisted PEC and colorimetric dual-signal biosensor by integrating the aptamer-induced HCR with the hydrolysate-induced vulcanization reaction of Bi_2MoO_6 nanosheets (Figure 9) [62]. The target-aptamer interaction could cause the release of trigger DNA (tDNA) from the tDNA/aptamer hybrid. The released tDNA was then captured by the anchor DNA (aDNA)-modified MB through hybridization reaction, thus initiating the HCR in the presence of two biotinylated hairpin DNA probes and leading to the formation of a long dsDNA on the MB surface. Then, the abundant SA-ALP conjugates were anchored on the MB by binding with the biotin tags. The captured ALP catalyzed the hydrolysis of sodium thiophosphate (TP) to produce H_2S. The resulting H_2S could react with Bi_2MoO_6 (BMO) to produce vulcanized BMO (BMO-S), thus leading to the enhancement of PEC signal. Meanwhile, the solution color changed from light yellow to brown. In addition, Qiu et al. reported the Ti_3C_2 MXene-anchored PEC detection of exosomes, in which ALP catalyzed the in-situ production of S^{2-} that could react with Cd^{2+} to form CdS on the surface of MXene, leading to an elevated photocurrent [63]. Li et al. employed hemin/G-quadruplex complexes with HRP-like activity to catalyze the conversion of $Na_2S_2O_3$ into H_2S that could further react with BiOBr nanoflowers on the electrode, thus producing a strong PEC signal [64]. Zeng et al. reported a PEC biosensor for miRNA-21 detection by combining the catalytic hairpin assembly-mediated CRISPR-Cas12a system and HRP catalysis [65]. In this work, the HRP-catalytic product of benzo-4-chlorohexadienone (4-CD) precipitating on the photoactive matrix yolk-in-shell Au@CdS acted as the signal quencher to cause the decrease of photocurrent.

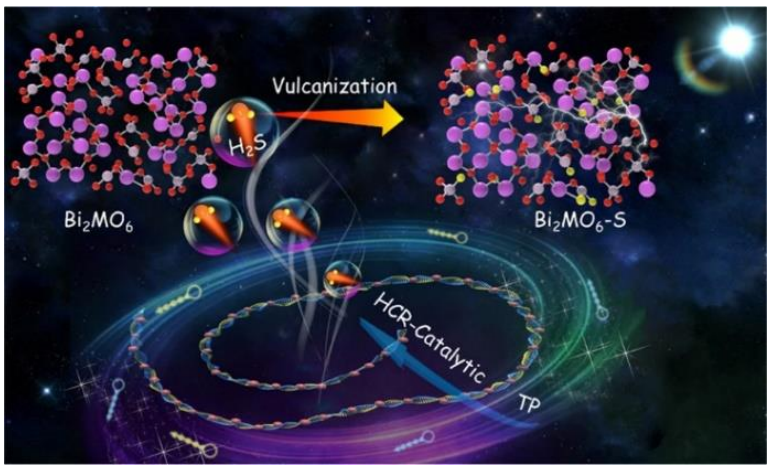

Figure 9. Schematic illustrations for a PEC-colorimetry dual-response biosensing plarform for the detection of PSA by coupling ALP-based signal amplification tool and BMO as the multifunctional signal indicator. Reproduced with permission [62]. Copyright 2021, American Chemical Society.

2.3 Signal labels

Nanozymes have attracted intense interest due to their low cost and high stability. Ferromagnetic (Fe_3O_4) nanoparticles with peroxidase-like activity have been used as the signal amplifiers in PEC biosensors. For example, Li et al. developed a PEC immunosensor with Fe_3O_4 nanozyme as the signal

reporter [66]. The ITO electrode modified with ZnO nanorods (ZnO-NRs) and $ZnIn_2S_4$ nanocrystals was used to immobilize the capture antibody. After the sandwich immunoreaction, the Fe_3O_4 nanozyme caused the production of insoluble and insulating precipitates, thus decreasing the photocurrent. Wei et al. developed a visible-light driven PEC immunosensor for the detection of microcystin-LR by using HRP and Ab_2-modified Fe_3O_4@PDA as the labels [67]. In this study, Fe_3O_4 nanoparticles and HRP synergistically catalyzed the generation of 4-CD that could precipitate on the surface of modified electrode to decrease the current intensity.

According to the previous reports, the extra magnetic field can promote the separation of photoinduced electons/holes and suppress the combination of charge carriers [68-70]. Thus, magnetic photoactive materials have been integrated with PEC bioassays. For example, Cheng et al. reported a microfluidic ratiometric magnetic-PEC (M-PEC) biosensor by using $ZnFe_2O_4$@Ag_2O as the magnetic photoactive tag [71]. As shown in Figure 10, the Bi_2WO_{6-x}/amorphous BiOCl nanosheets/Bi_2S_3 (p-BWO-s) were used as the photochromic color centers. After the immunoreaction, the Ab_2-modified $ZnFe_2O_4$@Ag_2O caused the decrease of the photocurrent response through the steric hindrance effect and the competitive consume of AA. Moreover, the presence of the magnetic field could result in the further decrease of the PEC signal.

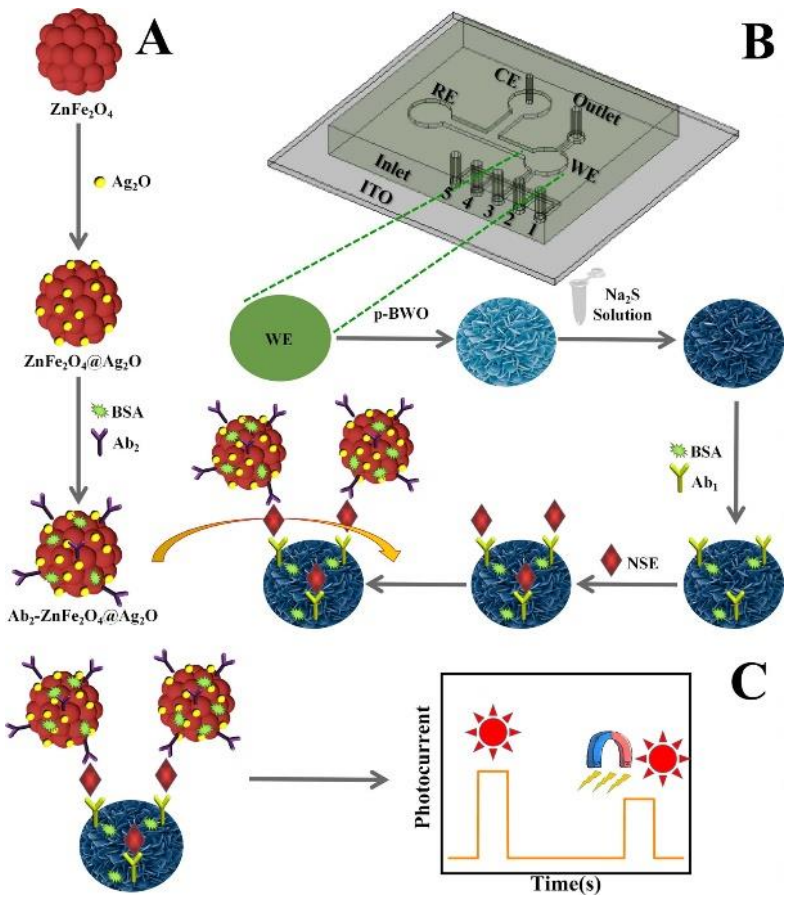

Figure 10. Schematic illustrations for (A) preparation process of Ab_2-$ZnFe_2O_4$@Ag_2O, (B) construction procedure for the sensing zone of microfluidic ratiometric M-PEC biosensor, and (C) testing process for the biosensor. Reproduced with permission [71]. Copyright 2021, American Chemical Society.

Recently, the lab-on-paper PEC bioanalysis devices have been broadly developed in the point-of-care testing field. To improve the reliability of the assays, methods with dual-signal and universal capability are more attractive. Li and co-workers reported a thermoresponsive and PEC dual-signal sensing platform for miRNA detection by transferring Fe_3O_4 nanoparticles into Prussian blue nanoparticles (PB NPs) (Figure 11) [72]. In this work, the spatially separable photothermal agent was used as the light-to-heat energy transducer and the $CuInS_2/CoIn_2S_4$ composite was used as the photoelectric converter in the lab-on-paper. The target could trigger the release of Fe_3O_4 NPs via the enzyme-assisted strand displacement cycle strategy. Meanwhile, the released Fe_3O_4 NPs were moved to the photothermal zone containing an acidic material through a hydrophilic bridge and then transformed into PB NPs with photothermal property and special color. Under the NIR/visible light irradiation, the temperature increased with the recovery of PEC signal.

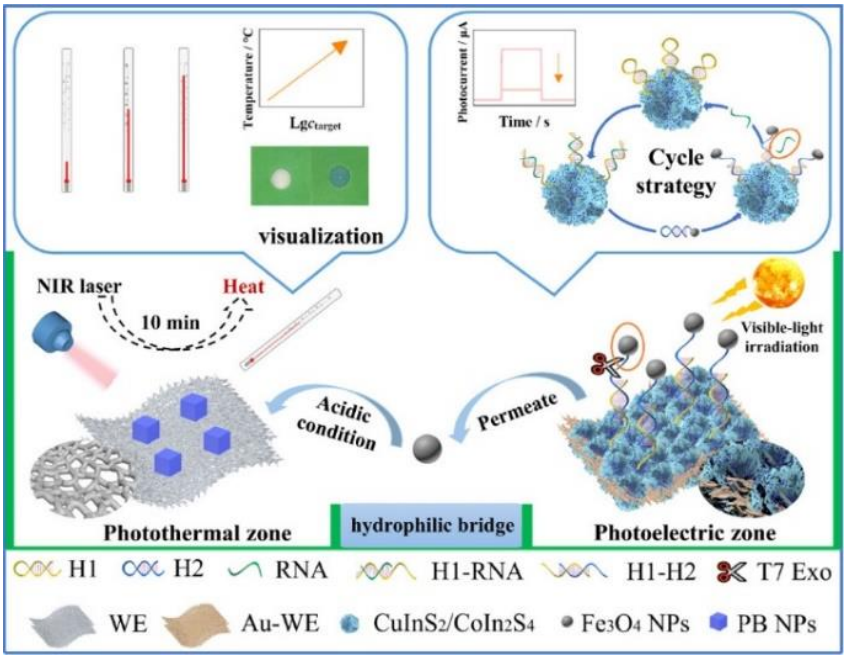

Figure 11. Schematic illustrations for the lab-on-paper thermoresponsive-photoelectric sensor. Reproduced with permission [72]. Copyright 2022, American Chemical Society.

Table 3. Detection performances of different PEC biosensors by using MBs as signal labels.

Signal labels	Target	Linear range	LOD	Ref.
His-Fe_3O_4	PSA	50 fg/mL ~ 1 ng/mL	18 fg/mL	[66]
Fe_3O_4@PDA@HRP	microcystin-LR	0.005 ~ 500 μg/L	0.001 μg/L	[67]
$ZnFe_2O_4$@Ag_2O	NSE	100 fg/mL ~ 100 ng/mL	33 fg/mL	[71]
Fe_3O_4	microRNA-141	0.5 pM ~ 2 nM	0.29 pM	[72]

Abbreviation: His, histidine; PSA, prostate-specific antigen; PDA, polydopamine; HRP, horseradish peroxidase; NSE, neuron-specific enolase antigen.

3. CONCLUSION

In this work, we summarized the progress in the design and application of magnetic-assisted PEC biosensors. The analytical performances including the detection limit and linear range and the functions of magnetic materials in the sensing systems were discussed. In general, the magnetic materials can be used as the carries to capture and concentrate the targets or load the signal reporters. The magnetic-assisted homogeneous reaction and target conversion have promoted the progress in the design and practical application of PEC biosensors. This work should be valuable for the development of effective and high-throughput PEC biosensors to detect different biomarkers.

ACKOWLEDGMENTS
This work was supported by the Science and Technology Development Program of Henan province (No. 222102320057).

References

1. Q. Zhou and D. Tang, *TrAC-Trend. Anal. Chem.*, 124 (2020) 115814.
2. W. W. Zhao, J. J. Xu and H. Y. Chen, *Int. J. Electrochem. Sci.*, 114 (2014) 7421.
3. Y. Feng, H. Xie and B. Zhou, *Int. J. Electrochem. Sci.*, 17 (2022) 220641.
4. L. Hou, B. Zhou, Y. Li and M. La, *Int. J. Electrochem. Sci.*, 14 (2019) 4453.
5. T. Kavetskyy, M. Alipour, O. Smutok, O. Mushynska, A. Kiv, D. Fink, F. Farshchi, E. Ahmadian and M. Hasanzadeh, *Microchem. J.*, 167 (2021) 106320.
6. L. Wang and J. Lin, *TrAC-Trend. Anal. Chem.*, 128 (2020) 115915.
7. N. Xia, D. Wu, H. Yu, W. Sun, X. Yi and L. Liu, *Talanta*, 221 (2021) 121640.
8. F. Li, S. Wang, H. Yin, Y. Chen, Y. Zhou, J. Huang and S. Ai, *ACS Sens.*, 5 (2020) 1092.
9. N. Xia, D. Deng, X. Mu, A. Liu, J. Xie, D. Zhou, P. Yang, Y. Xing and L. Liu, *Sens. Actuat. B: Chem.*, 306 (2020) 127571.
10. N. Xia, D. Wu, T. Sun, Y. Wang, X. Ren, F. Zhao, L. Liu and X. Yi, *Sens. Actuat. B: Chem.*, 327 (2021) 128913.
11. Y. Chen, Y. Zhou, H. Yin, F. Li, H. Li, R. Guo, Y. Han and S. Ai, *Sens. Actuat. B: Chem.*, 307 (2020) 127633.
12. S. T. Shanmugam, S. Trashin and K. De Wael, *Biosens Bioelectron*, 195 (2022) 113652.
13. H. Li, Y. Li, J. Li, F. Yang, L. Xu, W. Wang, X. Yao and Y. Yin, *Anal. Chem.*, 92 (2020) 4094.
14. Q. Zeng, Q. Wei, J. Luo, Y. Qian, M. Yang, Y. Zou and L. Lu, *Chin. Chem. Lett.*, 33 (2022) 2954.
15. J. Li, Y. Li, L. Xu, X. Fang, H. Yin, Q. Xu, H. Fang, H. Li and W. Wang, *Sens. Actuat. B: Chem.*, 320 (2020) 128597.
16. Y. Chen, L. Xu, Q. Xu, Y. Wu, J. Li and H. Li, *Biosens. Bioelectron.*, 215 (2022) 114569.
17. F. Mo, M. Han, X. Weng, Y. Zhang, J. Li and H. Li, *Anal. Chem.*, 93 (2021) 1764.
18. J. Luo, Q. Zeng, S. Liu, Q. Wei, Z. Wang, M. Yang, Y. Zou and L. Lu, *Sens. Actuat. B: Chem.*, 363 (2022) 131814.
19. Z. Wang, J. Luo, M. Yang and X. Wang, *Anal. Bioanal. Chem.*, 413 (2021) 5259.
20. J. Luo, D. Liang, D. Zhao and M. Yang, *Biosens. Bioelectron.*, 151 (2020) 111976.
21. J. Luo, D. Liang, X. Li, S. Liu, L. Deng, F. Ma, Z. Wang, M. Yang and X. Chen, *Microchim. Acta*, 188 (2021) 166.
22. L. Chen, J. Tong and M. Yang, *Mater Lett*, 305 (2021) 130798.
23. Z. Yu, H. Gong, Y. Li, J. Xu, J. Zhang, Y. Zeng, X. Liu and D. Tang, *Anal. Chem.*, 93 (2021) 13389.

24. J. Li, L. Xu, Y. Shen, L. Guo, H. Yin, X. Fang, Z. Yang, Q. Xu and H. Li, *Anal. Chem.*, 92 (2020) 8607.
25. C. Ding, K. Song, H. Meng, B. Zhang, Z. Zhao, H. Chang and W. Wei, *Microchim. Acta*, 185 (2018) 530.
26. Y. Lin, Q. Zhou and D. Tang, *Anal. Chem.*, 89 (2017) 11803.
27. H. Gong, Y. Wu, R. Zeng, Y. Zeng, X. Liu and D. Tang, *Chem. Commun.*, 57 (2021) 8977.
28. J. Zhang, Y. Gao, X. Zhang, Q. Feng, C. Zhan, J. Song, W. Zhang and W. Song, *Anal. Chem.*, 93 (2021) 7242.
29. R. Zeng, L. Zhang, Z. Luo and D. Tang, *Anal. Chem.*, 91 (2019) 7835.
30. D. Luo, Q. Fu, R. Gao, L. Su, Y. Su and B. Liu, *Anal. Bioanal. Chem.*, 414 (2022) 3033.
31. Y. Zhao, L. Tan, X. Gao, G. Jie and T. Huang, *Biosens. Bioelectron.*, 110 (2018) 239.
32. Y. Xia, T. Chen, W. Chen, G. Chen, L. Xu, L. Zhang, X. Zhang, W. Sun, J. Lan, X. Lin and J. Chen, *Anal. Chim. Acta*, 1191 (2022) 339279.
33. Z. Qiu, J. Shu and D. Tang, *Anal. Chem.*, 90 (2018) 1021.
34. S. Lv, K. Zhang, Q. Zhou and D. Tang, *Sens. Actuat. B: Chem.*, 310 (2020) 127874.
35. S. Lv, K. Zhang, L. Zhu and D. Tang, *Anal. Chem.*, 92 (2020) 1470.
36. J. Lei, B. Han, S. Lv, Y. Li, J. Tang, Y. Mao and J. Zhuang, *Electrochem. Commun.*, 92 (2018) 43.
37. K. Zhang, S. Lv, M. Lu and D. Tang, *Biosens. Bioelectron.*, 117 (2018) 590.
38. K. Zhang, S. Lv and D. Tang, *Anal. Chem.*, 91 (2019) 10049.
39. H. Li, M. Han, X. Weng, Y. Zhang and J. Li, *ACS Nano*, 15 (2021) 1710.
40. Q. Zhu, P. Yang, C. Zhu, Y. He, L. Fang, H. Huang, C. Li, L. Wang, J. Deng, Y. Li and J. Zheng, *Sens. Actuat. B: Chem.*, 364 (2022) 131920.
41. H. Yuan, J. Sun, Q. Zhang, M. Chu, G. Cheng, X. Li and Q. Xue, *Analyst*, 147 (2022) 3415.
42. Y. Fu, K. Xiao, Q. Zhang, X. Zhang, C. Du and J. Chen, *Anal. Chem.*, 94 (2022) 1874.
43. X. Niu, C. Lu, D. Su, F. Wang, W. Tan and F. Qu, *Anal. Chem.*, 93 (2021) 13727.
44. L. Y. Xia, M. J. Li, H. J. Wang, R. Yuan and Y. Q. Chai, *Anal. Chem.*, 92 (2020) 14550.
45. J. Li, X. Weng, F. Mo, M. Han and H. Li, *Anal. Chem.*, 92 (2020) 15145.
46. T. Wu, M. Gui, Y. Cao, Y. Zhang, Z. Zheng, G. Xiao and H. Li, *Sens. Actuat. B: Chem.*, 357 (2022) 131402.
47. G. Wen, X. Yang and Y. Wang, *J. Mater. Chem. B*, 5 (2017) 7775.
48. H. Li, Y. Cao, T. Wu, Y. Zhang, Z. Zheng, J. Lv, A. Mao, Y. Zhang, Q. Tang and J. Li, *Anal. Chem.*, 93 (2021) 11043.
49. Q. Zhou, Y. Lin, K. Zhang, M. Li and D. Tang, *Biosens. Bioelectron.*, 101 (2018) 146.
50. Y. Li, W. Wang, H. Gong, J. Xu, Z. Yu, Q. Wei and D. Tang, *J. Mater. Chem. B*, 9 (2021) 6818.
51. Z. Yu, H. Gong, J. Xu, Y. Li, Y. Zeng, X. Liu and D. Tang, *Anal. Chem.*, 94 (2022) 3418.
52. Z. Yang, Y. Shi, W. Liao, H. Yin and S. Ai, *Sens. Actuat. B: Chem.*, 223 (2016) 621.
53. H. Gong, X. Hu, R. Zeng, Y. Li, J. Xu, M. Li and D. Tang, *Sens. Actuat. B: Chem.*, 369 (2022) 132307.
54. M. Hao, P. Miao, Y. Wang, W. Wang, S. Ge, X. Yu, X. X. Hu, B. Ding, J. Zhang and M. Yan, *Anal. Chem.*, 93 (2021) 11251.
55. J.-H. Zhu, M. Wang, L.-H. Tu, A.-J. Wang, X. Luo, L.-P. Mei, T. Zhao and J.-J. Feng, *Sens. Actuat. B: Chem.*, 347 (2021) 130553.
56. W. Huang, D. Zhan, Y. Xie, X. Li and G. Lai, *Biosens. Bioelectron.*, 197 (2022) 113708-113716.
57. R. Zeng and D. Tang, *Talanta*, 219 (2020) 121215.
58. Y. Lin, Q. Zhou, D. Tang, R. Niessner and D. Knopp, *Anal. Chem.*, 89 (2017) 5637.
59. K. Zhang, S. Lv, Q. Zhou and D. Tang, *Sens. Actuat. B: Chem.*, 307 (2020) 127631.
60. L. Su, Y. Song, C. Fu and D. Tang, *Anal. Chim. Acta*, 1052 (2019) 49.
61. J. Tang, J. Li, P. Xiong, Y. Sun, Z. Zeng, X. Tian and D. Tang, *Microchim. Acta*, 187 (2020) 450.
62. J. Xu, R. Zeng, L. Huang, Z. Qiu and D. Tang, *Anal. Chem.*, 94 (2022) 11441.

63. Z. Qiu, D. Fan, X. Xue, J. Zhang, J. Xu, H. Lyu and Y. Chen, *RSC Adv.*, 12 (2022) 14260-14267.
64. J. Li, P. Xiong, J. Tang, L. Liu, S. Gao, Z. Zeng, H. Xie, D. Tang and J. Zhuang, *Sens. Actuat. B: Chem.*, 331 (2021) 129451.
65. R. Zeng, J. Xu, L. Lu, Q. Lin, X. Huang, L. Huang, M. Li and D. Tang, *Chem. Commun.*, 58 (2022) 7562.
66. W. Li, G. C. Fan, F. Gao, Y. Cui, W. Wang and X. Luo, *Biosens. Bioelectron.*, 127 (2019) 64-71.
67. J. Wei, A. Qileng, Y. Yan, H. Lei, S. Zhang, W. Liu and Y. Liu, *Anal. Chim. Acta*, 994 (2017) 82.
68. J. Zhao, N. Li, R. Yu, Z. Zhao and J. Nan, *Chem. Engin. J.*, 349 (2018) 530.
69. X. Zhao, W. Gao, Q. Liu, C. Cui, W. Zhou, X. Wang, X. L. Zhang, L. Zhao, Y. Sang and H. Liu, *Chem. Engin. J.*, 404 (2021) 126972.
70. H. Xu, Y. Lin, T. Harumoto, J. Shi and C. Nan, *ACS Appl. Mater. Interfaces*, 9 (2017) 30127.
71. Q. Cheng, J. Feng, T. Wu, N. Zhang, X. Wang, H. Ma, X. Sun and Q. Wei, *Anal. Chem.*, 93 (2021) 13680.
72. L. Li, H. Yang, L. Li, X. Tan, S. Ge, L. Zhang, J. Yu and Y. Zhang, *ACS Sens.*, 7 (2022) 2429.